Adaptive Input-Output Linearization Technique for Robust Speed Control of Brushless DC Motor

Kyeong-Hwa Kim, In-Cheol Baik, Hyun-Soo Kim, and Myung-Joong Youn

Abstract

An adaptive input-output linearization technique for a robust speed control of a brushless DC (BLDC) motor is presented. By using this technique, the nonlinear motor model can be effectively linearized in Brunovski canonical form, and the desired speed dynamics can be obtained based on the linearized model. This control technique, however, gives an undesirable output performance under the mismatch of the system parameters and load conditions caused by the incomplete linearization. For the robust output response, the controller parameters will be estimated by a model reference adaptive technique where the disturbance torque and flux linkage are estimated. The adaptation laws are derived by the Popov's hyperstability theory and positivity concept. The proposed control scheme is implemented on a BLDC motor using the software of DSP TMS320C30 and the effectiveness is verified through the comparative simulations and experiments.

I. Introduction

In most servo controller designs using BLDC motors, the electrical dynamics are often neglected because the electrical dynamics are inherently faster than the associated mechanical dynamics. By neglecting the electrical dynamics, the current is usually considered as a control input for the BLDC motor drive system having the high gain current feedback, and the speed controller is designed based on the first-order linearized model by a field-oriented control. This results in the cascaded control structure where the inner-loop current control and the outer-loop speed control schemes are separately designed. Even though the speed controller can be simply designed by this control scheme, it also needs an additional current controller design [2, 3]. Thus, it is more efficient to directly design the speed controller without using a separate inner-loop current regulator. Furthermore, robotics, machine tools, and direct drive motors are characterized as a smaller degree of dynamic time scale separation [4]. For these high performance drive applications, a conventional cascaded speed controller can not assure a high dynamic performance and a sufficient accuracy over the entire operating range. The effective approach to cope with this limitation is to directly design the speed controller considering the whole nonlinear motor dynamics.

In recent years, feedback linearization techniques have been applied to the control of the nonlinear plants such as the robot manipulators, induction motors, and BLDC motors [5-10]. The main objective is to force the speed [7, 8] and torque [9] of an induction motor or the speed of a BLDC motor [10] to follow their reference trajectories. By using these control strategies, the nonlinear terms can be effectively canceled out, and the output error dynamics can be specified based on the linear design techniques [5]. These techniques, however, require the full knowledge of the system parameters and load conditions. In general, BLDC motor drive systems are faced with unavoidable and unmeasurable disturbances or some parameter variations. Coupling the load to the motor shaft may cause the variations of the inertia and viscous friction coefficient besides the load variation. Also, the flux linkage varies nonlinearly with the temperature rise. In [10], an input-output linearization technique has been applied for the speed control of a BLDC motor. In this scheme, an integral control has been introduced to improve the robustness against the inaccurate speed measurement. However, other motor parameter variations have not been considered. Even though a steady-state response can be improved by introducing the integral control, it cannot give a good transient response under the parameter variations.

In view of the robustness against a load variation, it is well known that the use of a disturbance observer is very effective [11]. However, there is still a problem of parameter uncertainty since the flux linkage is not exactly known for a disturbance observer. An adaptive load torque observer against the variation of the flux linkage of a BLDC motor has been designed by the gradient method [12]. However, the gradient method generally requires two supplementary assumptions, i.e., the initial values of

Manuscript received January 9, 1997; accepted April 17, 1997.

K. H. Kim, I. C. Baik, H. S. Kim, and M. J. Youn are with Department of Electrical Engineering Korea Advanced Institute of Science and Technology 373-1, Kusong-Dong, Yusong-Gu, Taejeon, 305-701, Korea.

the estimated parameters must be in the neighborhood of the true parameters and the speed of the adaptation must be low [13].

In this paper, a robust speed control strategy of a BLDC motor using an adaptive input-output linearization technique is presented. Under the assumption that the disturbance torque and flux linkage are unknown parameters, the input-output linearization is performed. The resultant model has the nonlinear disturbances in its input-output relation, which is caused by the unknown disturbance torque and the flux linkage variation. Applying the linear control law to such a model gives a steady-state output error as well as a deteriorated dynamic performance. To overcome these drawbacks, the disturbance torque and flux linkage will be estimated by using a model reference adaptive system (MRAS) technique and the adaptation laws are derived by the hyperstability theory and positivity concept. Since the nonlinear disturbances by the incomplete linearization can be effectively compensated by using this control scheme, a desired dynamic performance and a zero steady-state error can be obtained. The whole control processing is implemented by the software of DSP TMS320C30 for a BLDC motor driven by a three-phase voltage-fed PWM inverter.

II. Modeling of BLDC Motor

The stator voltage equations of a BLDC motor in the synchronous reference frame are described as follows [1]:

$$v_{qs}=R_s i_{qs}+L_s\, i_{qs}+L_s\omega_r i_{ds}+\lambda_m\omega_r \tag{1}$$

$$v_{ds}=R_s i_{ds}+L_s\, i_{ds}-L_s\omega_r i_{qs} \tag{2}$$

where R_s is the stator resistance, L_s is the stator inductance, ω_r is the electrical rotor angular velocity, and λ_m is the flux linkage established by the permanent magnet. The speed dynamics is expressed as

$$\dot{\omega_r}=\frac{3}{2}\frac{p^2}{J}\lambda_m i_{qs}-\frac{B}{J}\omega_r-\frac{p}{J}T_L \tag{3}$$

where J is the moment of inertia of the rotor and its attached load, B is the viscous friction coefficient, p is the number of pole pairs, and T_L is the load torque. Using ω_r, i_{qs}, and i_{ds} as the state variables, the nonlinear state equation of a BLDC motor can be expressed as follows:

$$\dot{x}=f(x)+g_1 v_{qs}+g_2 v_{ds} \tag{4}$$

where $x=[\,\omega_r\;\; i_{qs}\;\; i_{ds}\,]^T$, $g_1=\left(0\;\; \frac{1}{L_s}\;\; 0\right)^T$, $g_2=\left(0\;\; 0\;\; \frac{1}{L_s}\right)^T$

$$f(x)=\begin{pmatrix} \frac{3}{2}\frac{p^2}{J}\lambda_m i_{qs}-\frac{B}{J}\omega_r-\frac{p}{J}T_L \\ -\frac{R_s}{L_s}i_{qs}-\omega_r i_{ds}-\frac{\lambda_m}{L_s}\omega_r \\ -\frac{R_s}{L_s}i_{ds}+\omega_r i_{qs} \end{pmatrix}.$$

III. Controller Design Using Adaptive Input-Output Linearization Technique

1. *Modeling Considering Unknown Disturbance Torque and Flux Linkage Variation*

In appendix, the speed controller design method for a BLDC motor using the input-output linearization technique will be briefly explained. In the nominal condition of known parameters, a nonlinear motor model can be transformed to a linearized and decoupled form, and the speed tracking controller can be designed using the linear state feedback control law. Generally, to obtain the linear decoupled model, the full informations on the system parameters have to be known since the linearization under the mismatched parameters gives the incompletely linearized model including the nonlinear disturbances.

The effect of the variations of the inertia and viscous friction coefficient can be included in the disturbance torque. From the relationship between the developed torque and the mechanical load, the torque equation of the machine can be expressed using the nominal parameters as follows:

$$T_e=J_o\left(\frac{1}{p}\right)\frac{d\omega_r}{dt}+B_o\left(\frac{1}{p}\right)\omega_r+T_d \tag{5}$$

$$T_d=\Delta J\left(\frac{1}{p}\right)\frac{d\omega_r}{dt}+\Delta B\left(\frac{1}{p}\right)\omega_r+T_L \tag{6}$$

where $\Delta J=J-J_o$, $\Delta B=B-B_o$, subscript "o" denotes the nominal value, and T_d is the effective load disturbance. Using (5), the speed dynamics is expressed as

$$\dot{\omega_r}=\frac{3}{2}\frac{p^2}{J_o}\lambda_m i_{qs}-\frac{B_o}{J_o}\omega_r-\frac{p}{J_o}T_d. \tag{7}$$

Under the assumption that the disturbance torque and flux linkage are unknown parameters, (4) can be rewritten using the estimated values as follows:

$$\dot{x}=\hat{f}(x)+g_1 v_{qs}+g_2 v_{ds}+d_1\Delta T_d+d_2\Delta\lambda_m \tag{8}$$

where $\Delta T_d=T_d-\hat{T}_d$, $\Delta\lambda_m=\lambda_m-\hat{\lambda}_m$

$$d_1=\left(-\frac{p}{J_o}\;\; 0\;\; 0\right)^T,\quad d_2=\left(\frac{3}{2}\frac{p^2}{J_o}i_{qs}\;\; -\frac{\omega_r}{L_s}\;\; 0\right)^T$$

$$\hat{f}(x)=\begin{pmatrix} \frac{3}{2}\frac{p^2}{J_o}\hat{\lambda}_m i_{qs}-\frac{B_o}{J_o}\omega_r-\frac{p}{J_o}\hat{T}_d \\ -\frac{R_s}{L_s}i_{qs}-\omega_r i_{ds}-\frac{\hat{\lambda}_m}{L_s}\omega_r \\ -\frac{R_s}{L_s}i_{ds}+\omega_r i_{qs} \end{pmatrix}$$

and "^" denotes the estimated value.

2. Adaptive Input-output Linearization Technique

To linearize the nonlinear state equation in (8), the new state variables are defined as follows:

$$z_1 = h_1(x) = \omega_r \tag{9}$$

$$z_2 = L_{\mathcal{F}} h_1(x) = \frac{3}{2}\frac{p^2}{J_o}\hat{\lambda}_m i_{qs} - \frac{B_o}{J_o}\omega_r - \frac{p}{J_o}\hat{T}_d \tag{10}$$

$$z_3 = h_2(x) = i_{ds} \tag{11}$$

where z_1 is the speed, z_2 is the computed acceleration using the estimated parameter values, and z_3 is the d-axis current. The state z_2 is employed for the implementation of the linear control law instead of the real acceleration. As $\hat{\lambda}_m$ and $\hat{T}_d$ converge to their real values, z_2 converges to the real acceleration signal. By using (9)-(11) as the state variables, (8) can be rewritten as follows:

$$\dot{z}_1 = z_2 + L_{d1}h_1 \cdot \triangle T_d + L_{d2}h_1 \cdot \triangle\lambda_m \tag{12}$$

$$\dot{z}_2 = L_{\mathcal{F}}^2 h_1 + L_{g1}L_{\mathcal{F}} h_1 v_{qs} + \frac{d}{dt}\hat{T}_d \cdot L_{d1}h_1 + \frac{d}{dt}\hat{\lambda}_m \cdot L_{d2}h_1 + L_{d1}L_{\mathcal{F}} h_1 \triangle T_d + L_{d2}L_{\mathcal{F}} h_1 \triangle\lambda_m \tag{13}$$

$$\dot{z}_3 = L_{\mathcal{F}} h_2 + L_{g2}h_2 \cdot v_{ds} \tag{14}$$

where $L_{d1}h_1 = -\frac{p}{J_o}$

$$L_{d2}h_1 = \frac{3}{2}\frac{p^2}{J_o} i_{qs}$$

$$L_{g1}L_{\mathcal{F}} h_1 = \frac{3}{2}\frac{p^2}{J_o}\frac{\hat{\lambda}_m}{L_s}$$

$$L_{d1}L_{\mathcal{F}} h_1 = \frac{pB_o}{J_o^2}$$

$$L_{d2}L_{\mathcal{F}} h_1 = -\frac{3}{2}\frac{p^2}{J_o}\left(\frac{\hat{\lambda}_m}{L_s}\omega_r + \frac{B_o}{J_o} i_{qs}\right)$$

$$L_{\mathcal{F}} h_2 = -\frac{R_s}{L_s} i_{ds} + \omega_r i_{qs}$$

$$L_{\mathcal{F}}^2 h_1 = \frac{3}{2}\frac{p^2}{J_o}\hat{\lambda}_m\left(-\frac{R_s}{L_s} i_{qs} - \omega_r i_{ds} - \frac{\hat{\lambda}_m}{L_s}\omega_r\right) - \frac{B_o}{J_o}\left(\frac{3}{2}\frac{p^2}{J_o}\hat{\lambda}_m i_{qs} - \frac{B_o}{J_o}\omega_r - \frac{p}{J_o}\hat{T}_d\right).$$

To linearize the nonlinear equations in (12)-(14), the control input voltages v_{qs}^* and v_{ds}^* can be expressed as follows:

$$\begin{pmatrix} v_{qs}^* \\ v_{ds}^* \end{pmatrix} = D_a(x)^{-1}\begin{pmatrix} -L_{\mathcal{F}}^2 h_1 - \frac{d}{dt}\hat{T}_d \cdot L_{d1}h_1 - \frac{d}{dt}\hat{\lambda}_m \cdot L_{d2}h_1 + u_{a1} \\ -L_{\mathcal{F}} h_2 + u_{a2} \end{pmatrix} \tag{15}$$

where u_{a1} and u_{a2} are the linear control inputs which assign the output error dynamics, and the decoupling matrix $D_a(x)$ is defined as

$$D_a(x) = \begin{pmatrix} L_{g1}L_{\mathcal{F}} h_1 & 0 \\ 0 & L_{g2}h_2 \end{pmatrix}. \tag{16}$$

Note that the estimated value $\hat{\lambda}_m$ is used in $D_a(x)$ for the calculation of $L_{g1}L_{\mathcal{F}} h_1$. In contrast to the non-adaptive case where $D(x)$ is always nonsingular, $D_a(x)$ becomes singular if the estimated flux linkage reaches a particular value. This value can be obtained using $detD_a(x) = 0$ as $\hat{\lambda}_m = 0$. This singularity has to be considered in the adaptation process. Everywhere except for this singular point, the control input voltages of (15) can be always obtained. Using (15), the nonlinear motor model becomes an incompletely linearized model and can be expressed as

$$\dot{z}_1 = z_2 + L_{d1}h_1 \cdot \triangle T_d + L_{d2}h_1 \cdot \triangle\lambda_m \tag{17}$$

$$\dot{z}_2 = u_{a1} + L_{d1}L_{\mathcal{F}} h_1 \cdot \triangle T_d + L_{d2}L_{\mathcal{F}} h_1 \cdot \triangle\lambda_m \tag{18}$$

$$\dot{z}_3 = u_{a2}. \tag{19}$$

Fig. 1 shows the block diagram of the resultant output dynamics after the linearization. As a result of the incomplete linearization due to the parameter deviations, the nonlinear disturbances exist in its input-output relation. Since such disturbances directly influence on the speed control performance such as a steady-state error and a large transient response, their effects must be quickly removed. Using the transformed state z, the linear control law is selected as follows:

$$u_{a1} = -k_{\omega 1}(z_1 - \omega_r^*) - k_{\omega 2}(z_2 - \dot{\omega}_r^*) + \ddot{\omega}_r^* \tag{20}$$

$$u_{a2} = -k_{id}(z_3 - i_{ds}^*) + \dot{i}_{ds}^*. \tag{21}$$

3. Estimations of disturbance torque and flux linkage

The disturbance torque and flux linkage will be simultaneously estimated using an MRAS technique to get a desired output

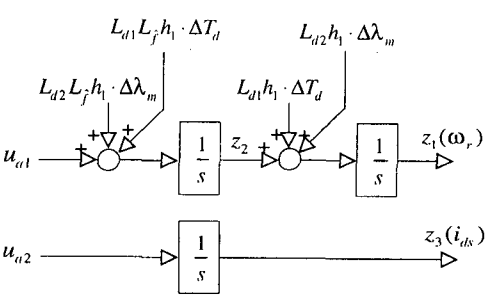

Fig. 1. Block diagram of the resultant incompletely linearized output dynamics.

dynamic performance. Using the linear decoupled model in (A11)-(A13) and the linear control law in (A14) and (A15), a reference model can be chosen as

$$\dot{z}_M = A_M z_M + U \tag{22}$$

where $z_M = [\, z_{1M} \;\; z_{2M} \;\; z_{3M}]^T$

$$A_M = \begin{pmatrix} 0 & 1 & 0 \\ -k_{\omega 1} & -k_{\omega 2} & 0 \\ 0 & 0 & -k_{id} \end{pmatrix}, \quad U = \begin{pmatrix} 0 \\ k_{\omega 1}\omega_r^* + k_{\omega 2}\dot{\omega}_r^* + \ddot{\omega}_r^* \\ k_{id} i_{ds}^* + \dot{i}_{ds}^* \end{pmatrix}.$$

This reference model represents a desired output dynamic behavior, which is resulted from imposing a linear control law on the linearized model under the assumption of the parameter matching. An adjustable model can be obtained from the incompletely linearized model in (17)-(19) and the corresponding linear control law in (20) and (21) as follows:

$$\dot{z} = A_M z + U + B_1 \cdot \Delta T_d + B_2 \cdot \Delta \lambda_m \tag{23}$$

where $B_1 = (\, L_{d1} h_1 \;\; L_{d1} L_{\mathcal{F}} h_1 \;\; 0)^T$, $B_2 = (\, L_{d2} h_1 \;\; L_{d2} L_{\mathcal{F}} h_1 \;\; 0)^T$.

The error between two models will be used to update the disturbance torque and flux linkage used in an adjustable model to reduce the output error. By subtracting the reference model from the adjustable model, the error dynamic equation can be obtained as follows:

$$\dot{\tilde{z}} = A_M \tilde{z} - W \tag{24}$$

where $\tilde{z} = z - z_M$ and $W = -B_1 \cdot \Delta T_d - B_2 \cdot \Delta \lambda_m$. From this error dynamic equation, the adaptation mechanism can be defined as

$$v = P\tilde{z} \tag{25}$$

$$\hat{T}_d(v, t) = \int_0^t \Psi_1(v, t)\, d\tau + \Psi_2(v, t) + \hat{T}_d(0) \tag{26}$$

$$\hat{\lambda}_m(v, t) = \int_0^t \Phi_1(v, t)\, d\tau + \Phi_2(v, t) + \hat{\lambda}_m(0) \tag{27}$$

where P is a symmetric positive definite matrix, Ψ_1, Ψ_2, Φ_1, and Φ_2 are the nonlinear adaptation mechanisms for the estimations of the disturbance torque and flux linkage, and $\hat{T}_d(0)$ and $\hat{\lambda}_m(0)$ are the initial estimates. The design procedures to obtain the asymptotic adaptation become as follows:

1. Determine P, Ψ_1, Ψ_2, Φ_1, and Φ_2 such that $\lim_{t\to\infty} \tilde{z}(t) = 0$ for any initial conditions $z_M(0)$ and $z(0)$
2. Find the supplementary conditions which lead to $\lim_{t\to\infty} \hat{T}_d(v, t) = T_d$ and $\lim_{t\to\infty} \hat{\lambda}_m(v, t) = \lambda_m$.

Based on (24)-(27), an MRAS structure for the parameter estimations can be constructed as shown in Fig. 2, which consists of a

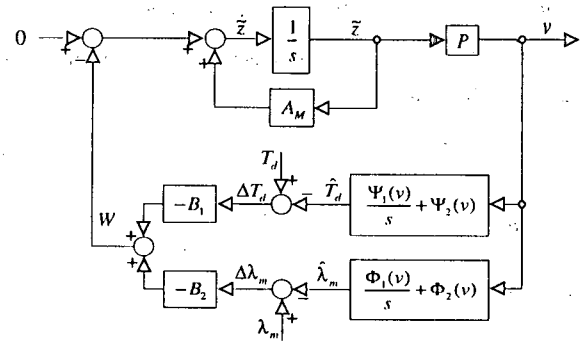

Fig. 2. Structure of MRAS for the estimations of the disturbance torque and flux linkage.

linear time invariant forward block and a nonlinear feedback block. This system is hyperstable if the forward transfer function matrix is strictly positive real and the input-output inner product of the nonlinear feedback block satisfies the Popov's integral inequality as follows [13]:

$$\int_0^{t_1} v^T W dt = \int_0^{t_1} (-v^T B_1 \cdot \Delta T_d - v^T B_2 \cdot \Delta \lambda_m) dt \geq -\gamma_o^2 \quad \text{for all } t_1 \geq 0 \tag{28}$$

where γ_o^2 is a finite positive constant. It is shown that for a given matrix A_n, the strictly positive real transfer function matrix

$$H(s) = P\,(sI - A_M)^{-1} \tag{29}$$

can be obtained by choosing P as the solution of the Lyapunov equation as follows:

$$A_M^T P + P A_M = -Q \tag{30}$$

where Q is a symmetric positive definite matrix [13]. If and only if the reference model is asymptotically stable, which is generally the case, (30) always has a positive definite matrix solution P.

To derive the adaptation mechanisms from (28), the estimated parameters need to be unknown constants or slowly-varying. Even though the disturbance torque T_d is not a constant parameter under the mechanical parameter variations such as the inertia and viscous friction coefficient, if the sampling interval is sufficiently fast as compared with the time variation of the unknown disturbance, T_d can be assumed to be a constant during each sampling intervals as follows [11-12]:

$$\frac{dT_d}{dt} = 0 \tag{31}$$

Using the above assumption, it is shown that the inequality in (28) can be satisfied by selecting the nonlinear adaptation mechanisms as follows [13]:

$$\Psi_1 = k_{IT}(v^T B_1) \tag{32}$$

$$\Psi_2 = k_{PT}(v^T B_1) \tag{33}$$

$$\Phi_1 = k_{I\lambda}(v^T B_2) \tag{34}$$

$$\Phi_2 = k_{P\lambda}(v^T B_2) \tag{35}$$

where k_{PT} and k_{IT} are the PI gains for the disturbance torque estimation, respectively, and $k_{P\lambda}$ and $k_{I\lambda}$ are the PI gains for the flux linkage estimation, respectively. By substituting (32)-(35) into (26) and (27), the disturbance torque and flux linkage can be simultaneously estimated as follows:

$$\hat{T}_d(v,t) = \left(k_{PT} + \frac{k_{IT}}{s}\right) \cdot (v^T B_1) + \hat{T}_d(0) \tag{36}$$

$$\hat{\lambda}_m(v,t) = \left(k_{P\lambda} + \frac{k_{I\lambda}}{s}\right) \cdot (v^T B_2) + \hat{\lambda}_m(0) \tag{37}$$

with $v^T B_1 = v_1 \cdot L_{d1} h_1 + v_2 \cdot L_{d1} L_{\hat{f}} h_1$

$v^T B_2 = v_1 \cdot L_{d2} h_1 + v_2 \cdot L_{d2} L_{\hat{f}} h_1$

where $v = [\, v_1 \;\; v_2 \;\; v_3]^T$ and the nominal values T_{Lo} and λ_{mo} are used for the initial estimates of $\hat{T}_d(0)$ and $\hat{\lambda}_m(0)$, respectively.

Ⅳ. Simulations and Experiments

1. Configuration of Overall System

The overall block diagram for the proposed control scheme is shown in Fig. 3. The overall system consists of a reference model, an adjustable model, and an adaptation mechanism. In this figure, the large shaded area represents the adjustable model resulting from the parameter mismatch between the speed controller and motor, which is composed of a speed tracking controller, a PWM inverter, and a motor. During the operations, the transformed state z is continuously compared with the model output z_M. The difference $\tilde{z}$ is used in the adaptation mechanism to update the controller parameters used in the adjustable model. The computed reference voltage vector v_s^* are applied to a BLDC motor using the space vector PWM technique [14].

The configuration of the experimental system is shown in Fig. 4. The whole speed control algorithms including the space vector PWM technique are implemented by the assembly language program using DSP TMS320C30 with a clock frequency of 32 MHz. The sampling period is set to 128 [μsec] both in the simulations and experiments. The BLDC motor is driven by a three-phase PWM inverter employing the intelligent power module (IPM) with a switching frequency of 7.8 kHz. The rotor speed and absolute rotor position are detected through a 12 bit/rev resolver-to-digital converter (RDC) using a brushless resolver.

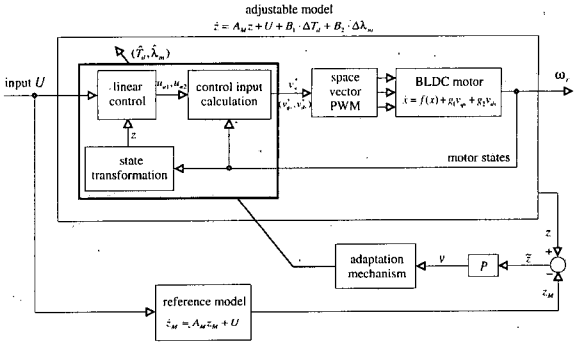

Fig. 3. Overall block diagram for the proposed control scheme.

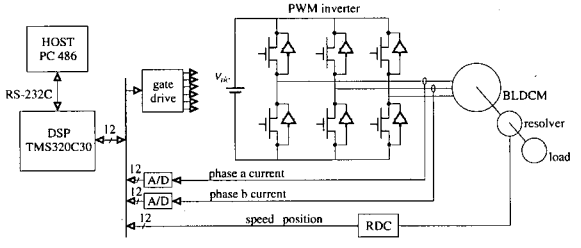

Fig. 4. Configuration of experimental system.

Table 1. Specifications of a BLDC motor.

Rated power	400 W	Rated speed	3000 rpm
Rated torque	1.274 Nm	Number of poles	4
Magnetic flux	0.17 Wb	Stator resistance	3.0 Ω
Stator inductance	10.5 mH	Moment of inertia	1.54×10^{-4} Nm · S^2

The nominal parameters of a BLDC motor are listed in Table 1.

2. Simulation Results

The d-axis current command is given as zero and the speed trajectory command is given as follows:

$$\omega_r^* = \frac{\omega_{rf}}{T} t - \frac{\omega_{rf}}{2\pi} \sin\left(\frac{2\pi t}{T}\right) \tag{38}$$

$$\dot{\omega}_r^* = \frac{\omega_{rf}}{T} - \frac{\omega_{rf}}{T} \cos\left(\frac{2\pi t}{T}\right) \tag{39}$$

$$\ddot{\omega}_r^* = 2\pi \frac{\omega_{rf}}{T^2} \sin\left(\frac{2\pi t}{T}\right) \tag{40}$$

where ω_{rf} is the desired final speed and T is the time when the speed command reaches from zero to ω_{rf}. Fig. 5 shows the output responses of the 2nd order linear control law in (20) and (21) without the adaptation algorithms. The gains of the linear control law are selected as $k_{\omega 2}$=140, $k_{\omega 1}$=9800, and k_{id}=1000 so that the poles of the speed error dynamics and the d-axis current

error dynamics are determined as $-70\pm i70$ and -1000, respectively. Under the nominal parameter values, the speed command can be well tracked. Also, the computed acceleration z_2 is effectively controlled to the acceleration command. However, the speed response shows an undesirable large transient error under the inertia variation. Furthermore, the computed acceleration z_2 becomes quite different from the acceleration command and the real acceleration obtained by the Euler's method. This is resulted from the calculation errors in both the control input voltages in (15) and the state z_2 in (10) due to the inertia variation. This can be improved by introducing the integral control action and disturbance observer [10]. However, the conventional disturbance observer requires the flux linkage to be known. Under the flux linkage variation, there exists an estimation error in the disturbance torque. Since this estimation error must be compensated by the integral action, the speed responses generally show large transients with a fixed integral gain. The speed responses for this case are shown in Fig. 6 Even under the inertia and load variations, the speed shows a good transient response and disturbance suppression with the nominal flux linkage since the disturbance observer estimates the effective disturbance torque.

However, under the flux linkage deviation, it is observed that the speed response shows the large transient and degraded disturbance suppression response. Thus, introducing the integrator and disturbance observer cannot be an effective way of improving the output dynamic performance under the flux linkage variation. Fig. 7 shows the speed transient responses for the proposed control scheme under the inertia variation. The flux linkage is

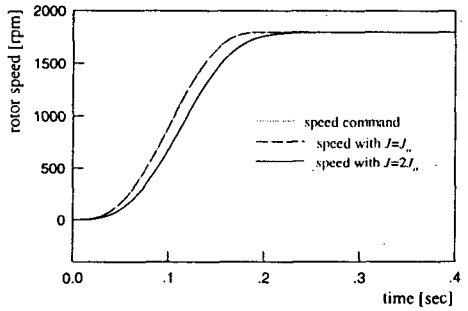

(a) speed transient response

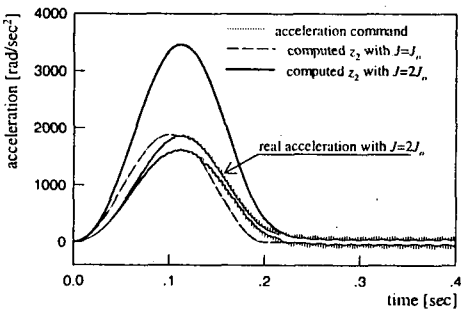

(b) acceleration response

Fig. 5. Output responses of the linear control law under the nominal parameters and inertia variation.

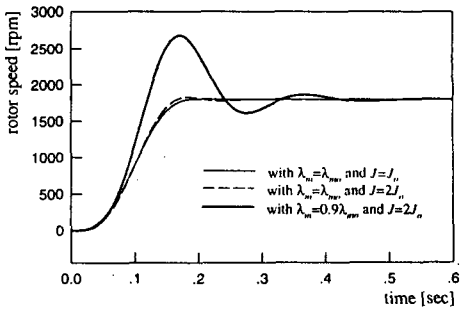

(a) speed transient responses under the flux linkage variation

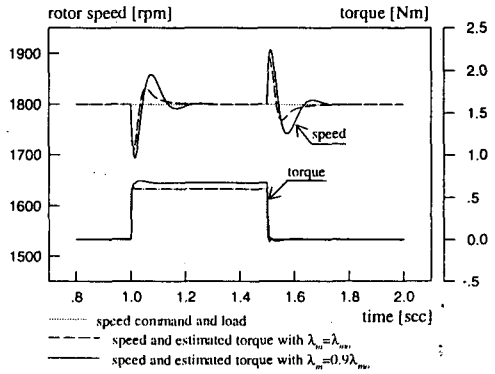

(b) disturbance suppression responses

Fig. 6. Speed responses of the linear control law with the integrator and load torque observer under the flux linkage variation.

assumed to be varied to 80% of its nominal value. The gains of the linear control law are set as the same as the non-adaptive case. The PI gains for the adaptation algorithms are chosen as follows: $k_{PT}=1\times10^{-4}$, $k_{IT}=5\times10^{-3}$, $k_{P\lambda}=0$, $k_{I\lambda}=3\times10^{-6}$, and $Q=diag(15\times10^{-3}\ 1)$. The adaptation algorithms start at t=0. As compared with Figs. 5(a) and 6(a), the speed response in Fig. 7(a) shows a high dynamic performance under both the flux linkage and inertia variations. This can be explained by the simultaneous estimations of the disturbance torque and flux linkage as shown in Fig. 7(b). It is noted that the disturbance torque estimator con-verges to $T_L+(\Delta J/p)\dot{\omega}_r$. This effectively suppresses the influence of the disturbance torque due to the inertia change on the speed dynamics. Fig. 7(c) shows the acceleration command $\dot{\omega}_r^*$, the real acceleration obtained from the Euler's method, and the computed acceleration signal z_2 using the estimated parameters. Unlike Fig. 5(b), as the real parameters are estimated, z_2 converges to the real acceleration signal and is effectively controlled to the acceleration command. Fig. 8 shows the output performance of the proposed control scheme when the step load torque is applied at t=0.3 [sec] and removed at t=0.5 [sec]. Similarly, the flux linkage is assumed to 80% of its nominal value. Under the presence of the flux linkage and load variations, the trajectory command can be well tracked. The maximum speed error due to the load change is less than 50 [rpm], and this error is rejected within 0.1 [sec]. Also, it

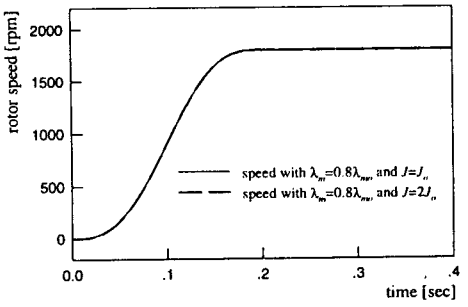

(a) speed transient responses

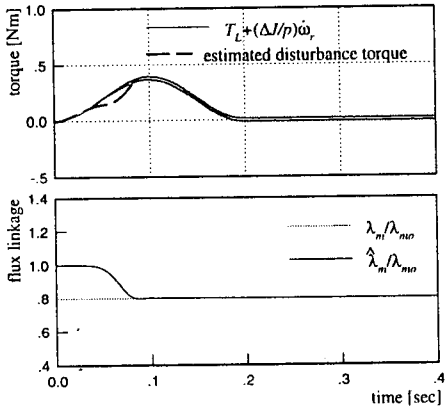

(b) parameter estimations with λ_m=0.8λ_{m0} and J=2J_0

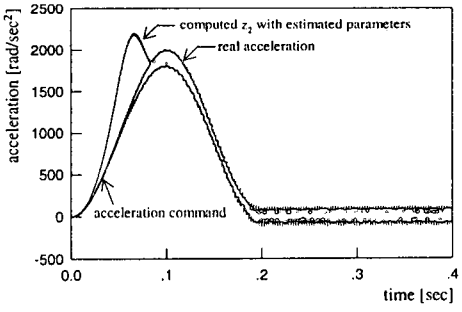

(c) acceleration response with λ_m=0.8λ_{m0} and J=2J_0

Fig. 7. Speed transient responses of the proposed control scheme under both the flux linkage and inertia variations.

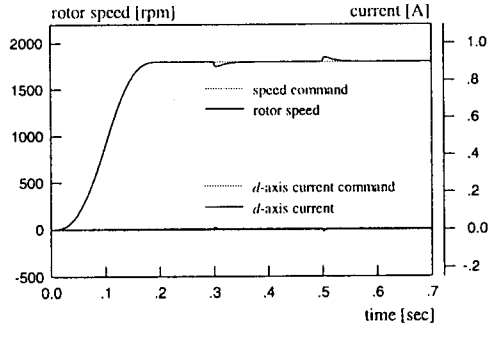

speed and d-axis current responses

Fig. 8. Output responses of the proposed control scheme under both the flux linkage and load variations (Step load torque of 0.6[Nm] is applied at t=0.3[sec] and removed at t=0.5[sec]).

can be shown that the d-axis current is well regulated to zero.

3. *Experimental Results*

In this section, the experimental results are presented to verify the feasibility of the proposed control scheme under the various conditions. For the performance comparison with the proposed control scheme, the 2nd order linear control law without the adaptation algorithms is used. The gains of the linear control law are the same as the simulation conditions. Fig. 9 shows the experimental results of the proposed control scheme when $\Delta\lambda_m$ is initially -20% of its nominal value. Since coupling the BLDC motor to a DC motor causes small parameter variations such as the inertia and viscous friction coefficient, the disturbance torque component due to the parameter mismatch is observed in the estimated disturbance torque. However, the speed response is unaffected by these variations and gives the desired dynamic performance and zero steady-state error. The computed acceleration z_2 using the estimated parameters shows a large transient error because of the flux linkage variation. However, as the flux linkage and disturbance torque are estimated, z_2 is well controlled to the acceleration command. The experimental results for the inertia variation are shown in Figs. 10-12. Without the adaptation algorithms, the speed response shows the undesirable dynamic performance under the inertia variation as shown in Fig. 10. Under both the flux linkage and inertia variations, the speed response shows the undesirable dynamic performance as well as

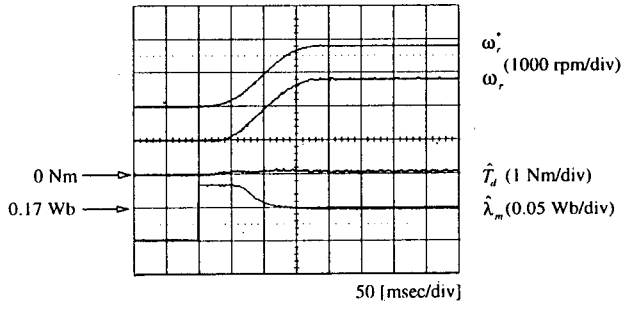

(a) speed transient response

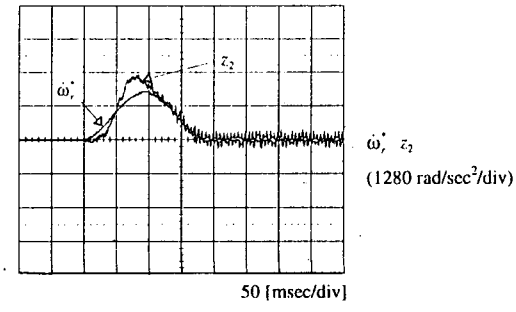

(b) computed acceleration using estimated parameters

Fig. 9. Experimental results of the proposed control scheme under the flux linkage variation.

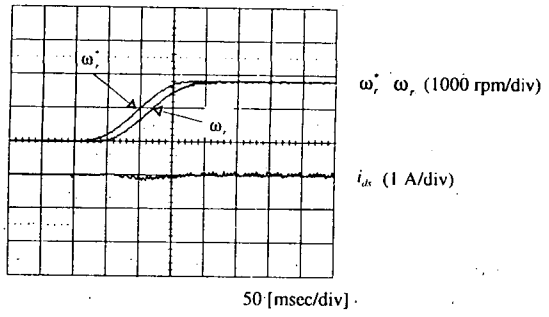

Fig. 10. Experimental results of the linear control law under the inertia variation without adaptation algorithms.

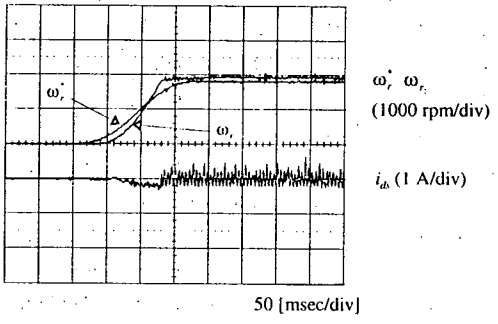

Fig. 11. Experimental results of the linear control law under both the flux linkage and inertia variations without adaptation algorithms.

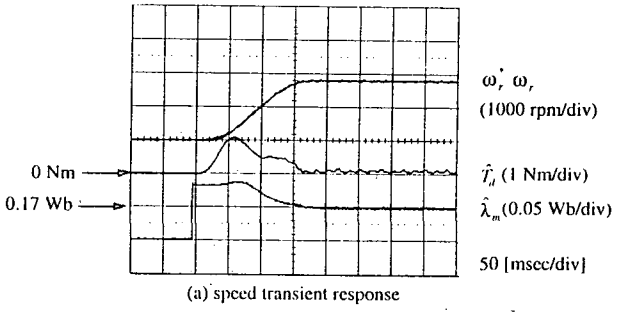

Fig. 12. Experimental results of the proposed control scheme under both the flux linkage and inertia variations.

the steady-state error as shown in Fig. 11. In the proposed scheme, however, the speed response shows a good dynamic performance well coincided with the simulation as a result of an effective simultaneous parameter estimations as shown in Fig. 12. Fig. 13 shows the disturbance suppression characteristics for both control schemes. The step load torque of 0.15 [Nm] is considered for a load variation, and the speed is operated at 2900 [rpm]. In the linear control law, a steady-state error of 70 [rpm] is observed in the speed response by a load change. On the contrary, this speed error is rejected within 0.1 [sec], and a good speed regulation is achieved in the proposed control scheme.

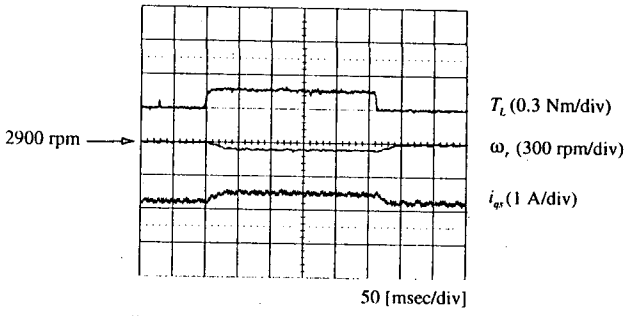

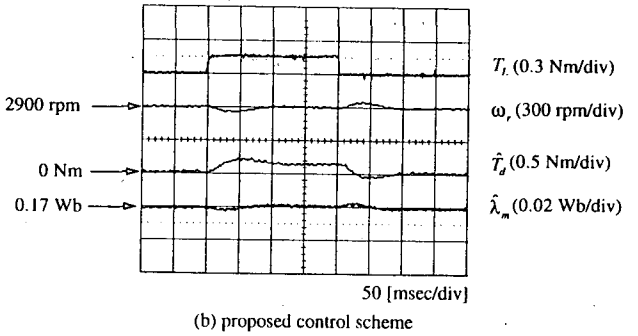

Fig. 13. Comparison of the disturbance suppression responses under the load variation.

V. Conclusions

An adaptive input-output linearization technique for a robust speed control of a BLDC motor has been proposed. By using this method, a systematic design approach for a speed controller can be accomplished without considering a separate inner-loop current regulator. Under the parameter variations, the input-output linearization scheme with the linear control law yields the steady-state errors as well as the deteriorated transient responses as a result of the incomplete linearization. In addition, introducing an integrator and a load torque observer cannot effectively deal with this problem. To overcome these limitations, the system parameters are estimated using an MRAS technique where the disturbance torque and the magnitude of the flux linkage can be simultaneously estimated. The estimated parameters are used for the input-output linearization to obtain a robust control performance. Thus, a speed control performance is not affected by the load torque disturbance and the variation of the motor and mechanical parameters. The whole control system is realized using the software of DSP TMS320C30 for a BLDC motor driven by a three-phase voltage-fed PWM inverter. Through the various comparative simulations and experimental results, it is verified that the proposed control scheme yields a robust output performance even under the presence of the variation of the motor parameter and the external disturbances caused by the inertia variation and step load change.

Ⅵ. Appendix
(Input-output feedback linearization)

To linearize the nonlinear model in (4), the controlled variable is differentiated with respect to time until the input appears. This can be easily done by introducing the Lie derivative of a state function $h(x)$: $R^n \rightarrow R$ along a vector field $f(x)=(f_1,\cdots,f_n)$ as follows [5]:

$$L_f h = \nabla h \cdot f = \sum_{i=1}^{n} \frac{\partial h}{\partial x_i} f_i(x) \tag{A1}$$

$$L_f^i h = L_f(L_f^{(i-1)} h). \tag{A2}$$

In order to avoid any zero dynamics, ω_r and i_{ds} are chosen as the outputs [10]. The objective of the control is to maintain the speed and d-axis current to their reference values or trajectories with the specified output dynamic performance. For this objective, the new state variables are defined as follows:

$$y_1 = h_1(x) = \omega_r \tag{A3}$$

$$y_2 = \dot{\omega_r} = L_f h_1(x) = \frac{3}{2}\frac{p^2}{J}\lambda_m i_{qs} - \frac{B}{J}\omega_r - \frac{p}{J}T_L \tag{A4}$$

$$y_3 = h_2(x) = i_{ds} \tag{A5}$$

where y_1 is the speed, y_2 is the acceleration, and y_3 is the d-axis current. The dynamic equations using the new state variables can be rewritten as follows:

$$\dot{y_1} = y_2 \tag{A6}$$

$$\dot{y_2} = L_f^2 h_1 + L_{g1} L_f h_1 \cdot v_{qs} \tag{A7}$$

$$\dot{y_3} = L_f h_2 + L_{g2} h_2 \cdot v_{ds} \tag{A8}$$

where $L_{g1}L_f h_1 = \frac{3}{2}\frac{p^2}{J}\frac{\lambda_m}{L_s}$

$$L_f h_2 = -\frac{R_s}{L_s} i_{ds} + \omega_r i_{qs}$$

$$L_{g2} h_2 = \frac{1}{L_s}$$

$$L_f^2 h_1 = \frac{3}{2}\frac{p^2}{J}\lambda_m\left(-\frac{R_s}{L_s} i_{qs} - \omega_r i_{ds} - \frac{\lambda_m}{L_s}\omega_r\right).$$

$$-\frac{B}{J}\left(\frac{3}{2}\frac{p^2}{J}\lambda_m i_{qs} - \frac{B}{J}\omega_r - \frac{p}{J}T_L\right).$$

To linearize and decouple (A6)-(A8), the control input voltages v_{qs}^* and v_{ds}^* can be expressed as follows:

$$\begin{pmatrix} v_{qs}^* \\ v_{ds}^* \end{pmatrix} = D(x)^{-1}\begin{pmatrix} -L_f^2 h_1 + u_1 \\ -L_f h_2 + u_2 \end{pmatrix} \tag{A9}$$

where u_1 and u_2 are the new control inputs by which the desired output error dynamics can be assigned, and $D(x)$ is the decoupling matrix defined as

$$D(x) = \begin{pmatrix} L_{g1}L_f h_1 & 0 \\ 0 & L_{g2} h_2 \end{pmatrix}. \tag{A10}$$

Using (A9), the nonlinear state equations become a linear decoupled model of Brunovski canonical form as

$$\dot{y_1} = y_2 \tag{A11}$$

$$\dot{y_2} = u_1 \tag{A12}$$

$$\dot{y_3} = u_2. \tag{A13}$$

The above equations show the linear and decoupled relationship between the transformed states y and the new control inputs u. To assign the output error dynamics having the desired dynamic behavior, the new control inputs are designed by using a linear state feedback control law as follows:

$$u_1 = -k_{\omega 1}(y_1 - \omega_r^*) - k_{\omega 2}(y_2 - \dot{\omega}_r^*) + \ddot{\omega}_r^* \tag{A14}$$

$$u_2 = -k_{id}(y_3 - i_{ds}^*) + \dot{i}_{ds}^* \tag{A15}$$

where ω_r^* and i_{ds}^* are the commands for the speed and d-axis current, respectively. Then, this linear state feedback control gives the second order speed error dynamics and the first order d-axis current error dynamics. The desired poles can be easily chosen by adjusting the controller gains $k_{\omega 1}$, $k_{\omega 2}$, and k_{id} through the pole placement technique. This control scheme has some limitations. In order to implement the linear control law, the new state variables y must be available. It is, however, difficult to obtain the information on the acceleration since the acceleration signal cannot be easily measured and is very noisy. Thus, it has to be obtained from the original measured states x and motor parameters using (A4). If there are some parameter variations or uncertainties on the model, these will cause errors in the transformation into the new state y as well as in the computation of the control input voltages in (A9), which results in the output speed error.

References

[1] P. C. Krause, Analysis of Electric Machinery, McGraw-Hill, New York, 1986.

[2] D. M. Brod, and D. W. Novotny, Current control of VSI-PWM inverters, IEEE Trans. Industry Applications, Vol. 21, No. 4, pp. 562-570, March/April 1985.

[3] K. Y. Cho, J. D. Bae, S. K. Chung, and M. J. Youn, Torque harmonics minimisation in permanent magnet synchronous

motor with back EMF estimation, IEE Proc. Electr. Power Appl. Vol. 141, No. 6, pp. 323-330, 1994.

[4] J. J. Carroll Jr., and D. M. Dawson, Integrator backstepping techniques for the tracking control of permanent magnet brush dc motors, IEEE Trans. Industry Applications, Vol. 31, No. 2, pp. 248-255, March/April 1995.

[5] J. J. E. Slotine, and W. Li, Applied Nonlinear Control, Prentice-Hall International Editions, 1991.

[6] P. D. Olivier, Feedback linearization of dc motors, IEEE Trans. Industrial Electronics, Vol. 38, No. 6, pp. 498-501, Nov. 1991.

[7] A. Bellini, G. Figalli, and F. Tosti, Linearized model of induction motor drives via nonlinear state feedback decoupling, in Proceedings of European Power Electronics Conference, Firenze, pp. 36-41, 1991.

[8] T. von Raumer, J. M. Dion, L. Dugard, and J. L. Thomas, Applied nonlinear control of an induction motor using digital signal processing, IEEE Trans. Control System Technology, Vol. 2, No. 4, pp. 327-335, Dec. 1994.

[9] L. A. Pereira, and E. M. Hemerly, Design of an adaptive linearizing control for induction motors, IEEE IECON 95 conference record, pp. 1012-1016, 1995.

[10] B. Le Pioufle, Comparison of speed nonlinear control strategies for the synchronous servomotor, Electric Machines and Power Systems, Vol. 21, pp. 151-169, 1993.

[11] N. Matsui, T. Makino, and H. Satoh, Autocompensation of torque ripple of direct drive motor by torque observer, IEEE Trans. Industry Applications, Vol. 29, No. 1, pp. 187-194, Jan./Feb. 1993.

[12] J. S. Ko, J. H. Lee, and M. J. Youn, Robust digital position control of brushless DC motor with adaptive load torque observer, IEE Proc. Electr. Power Appl. Vol. 141, No. 2, pp. 63-70, 1994.

[13] Y. D. Landau, Adaptive Control-The Model Reference Approach, Marcel Dekker, New York, 1979.

[14] H. W. van der Broeck, H. C. Skudelny, and G. V. Stanke, Analysis and realization of a pulsewidth modulator based on voltage space vectors, IEEE Trans. Industry Applications, Vol. IA-24, No. 1, pp. 142-150, Jan./Feb. 1988.

Kyeong-Hwa Kim was born in Seoul, Korea, on March 11, 1969. He received the B.S. degree in Electrical Engineering from Han-Yang University, Seoul, Korea, in 1991, and the M.S. degree in Electrical Engineering from Korea Advanced Institute of Science and Technology(KAIST), Taejon, Korea, in 1993. He is currently working toward the Ph.D. Degree in Electrical Engineering at KAIST. His research interests are in the areas on power electronics and control, which includes are machine drives and micropocessor-based control applications.

Hyun-Soo Kim was born in Kyoungbuk, Korea, on December 1, 1972. He received the B.S. and M.S. degrees in Electrical Engineering from Korea Advanced Institute of Science and Technology(KAIST), Taejon, Korea, in 1994 and 1996, respectively. He is currently working toward the Ph.D. degree in Electrical Engineering at KAIST. His research interests are in the areas on power electronics and control, which includes ac machine drives and microprocessor-based control applications.

In-Cheol Baik was born in Seoul, Korea, on February 25, 1962. He received the B.S. degree in elelctronics form Konkuk University in 1984 and the M.S. degree in electrical engineering from the Korea Advanced Institute of Science and Technology(KAIST) in 1987. He was a recipient of the University scholarship from Konkuk University during 1980-1982. He has been with the Living system research laboratory of LG Electronics Inc., Seoul from 1987. From February to May 1990, he took the Application Engineer course at Siemens Energy & Automation Training Center, Manchester, U.K. Since March 1993, he has been a Ph.D. student in the department of electrical engineering at KAIST. His research interests include rotating electrical machine drive systems, power converters, and control engineering.

Myung-Joong Youn was born in Seoul, Korea, on November 26, 1946. He received the B.S. degree from Seoul National University, Seoul, Korea, in 1970, and the M.S. and Ph.D. degrees in electrical engineering from the Univeristy of Missouri-Columbia in 1974 and 1978, respectively. He was with the Air-craft Equimpment Division of General Electric Company at Erie, Pennsylvania, since 1978, where he was as Individual Contributor on Aerospace Electrical Engineering. Korea Advanced Institute of Science and Technology since 1983 where he is now a professor. His research activities are in the areas on power electronics and controll which include the drive system, rotating electrical machine design, and high-performance switching regulators. Dr. Youn is a member of KIEE and KITE.